GDCh Research Article Angewandte International Edition Chemie www.angewandte.org

How to cite: *Angew. Chem. Int. Ed.* **2024**, *63*, e202408622
doi.org/10.1002/anie.202408622

Rotational Spectroscopy | Hot Paper

Structural and Electronic Evolution of Ethanolamine upon Microhydration: Insights from Hyperfine Resolved Rotational Spectroscopy

Fan Xie, Marco Mendolicchio, Wafaa Omarouayache, S. Indira Murugachandran, Juncheng Lei, Qian Gou, M. Eugenia Sanz,* Vincenzo Barone,* and Melanie Schnell**

Abstract: Ethanolamine hydrates containing from one to seven water molecules were identified via rotational spectroscopy with the aid of accurate quantum chemical methods considering anharmonic vibrational corrections. Ethanolamine undergoes significant conformational changes upon hydration to form energetically favorable hydrogen bond networks. The final structures strongly resemble the pure $(H_2O)_{3-9}$ complexes reported before when replacing two water molecules by ethanolamine. The ^{14}N nuclear quadrupole coupling constants of all the ethanolamine hydrates have been determined and show a remarkable correlation with the strength of hydrogen bonds involving the amino group. After addition of the seventh water molecule, both hydrogen atoms of the amino group actively contribute to hydrogen bond formation, reinforcing the network and introducing approximately 21–27 % ionicity towards the formation of protonated amine. These findings highlight the critical role of microhydration in altering the electronic environment of ethanolamine, enhancing our understanding of amine hydration dynamics.

Introduction

Water impacts molecular structures and reactivities in many chemical and biomolecular processes[1–5] through mechanisms such as hydrophobic interactions and the formation of hydration shells. Investigating the structure of hydrates at the microscopic level enables isomer-specific identification of hydrogen bonding networks and elucidates size-dependent reactivity that bridges to macroscopic properties of matter. This can advance our understanding on various phenomena, such as the growth and aging of aerosol particles in the Earth's atmosphere,[6,7] and the hydration enhanced conformational stability of proteins and oligonucleotides,[8–10] etc.

In this endeavor, spectroscopic studies of small water clusters and gas-phase water-solute aggregates, considered as fundamental building blocks of aqueous environments,[11,12] have yielded extensive results. In particular, microwave (MW) spectroscopy, aided by quantum chemical (QC) calculations, has been pivotal in characterizing hydrogen bond networks. Pioneering studies on pure water clusters revealed two-dimensional cyclic arrangements in smaller clusters of $(H_2O)_{3-5}$, transitioning to three-dimensional networks in $(H_2O)_6$, which displays different isomers with prism, cage, and book structures. Subsequently, the characterizations of $(H_2O)_{7-10}$ highlighted that cooperative and many-body interactions significantly enhance the strength of hydrogen bonds resulting in reinforced networks.[13–20]

In the last decade, MW spectroscopic studies have been increasingly focused on the exploration of microhydration effects and water-solute interactions in larger organic-water clusters, involving up to seven water molecules.[21–28] These studies showed how water configurations and the corresponding hydrogen bond networks adapt to the solute to optimize interactions. The observation of ^{18}O and D

[*] Dr. F. Xie, Prof. Dr. M. Schnell
Deutsches Elektronen-Synchrotron DESY, Notkestr. 85, 22607 Hamburg, Germany
E-mail: melanie.schnell@desy.de
Prof. Dr. M. Schnell
Institut für Physikalische Chemie, Christian-Albrechts-Universität zu Kiel, Max-Eyth-Str. 1, 24118 Kiel, Germany
Dr. M. Mendolicchio
Scuola Normale Superiore, piazza dei Cavalieri 7, 56125 Pisa, Italy
W. Omarouayache, Dr. S. I. Murugachandran, Dr. M. E. Sanz
Department of Chemistry, King's College London, London SE1 1DB, U.K.
E-mail: maria.sanz@kcl.ac.uk
J. Lei, Prof. Dr. Q. Gou
Department of Chemistry, School of Chemistry and Chemical Engineering, Chongqing Key Laboratory of Theoretical and Computational Chemistry, Chongqing University, 401331 Chongqing, China
E-mail: qian.gou@cqu.edu.cn
Prof. Dr. V. Barone
4INSTM, via G. Giusti 9, 50121 Firenze, Italy
E-mail: vincebarone52@gmail.com

monosubstituted isotopologues enabled the determination of structural parameters related to the hydrogen bond networks, including hydrogen and oxygen atom coordinates and O···O distances, with an accuracy to a few mÅ.[17,20,22,24,25,27,29] It has thus been possible to gauge changes in the O···O distances as the number of water molecules increases. Assessing changes in the hydrogen bond lengths themselves remains challenging due to the significant change in effective bond length from zero-point vibrational effects when substituting H with D.

The presence of a quadrupolar nucleus in the cluster, with nuclear spin $I > 1/2$, provides independent insight into the changes induced by complexation through an analysis of the additional hyperfine structure in the MW spectrum and the experimental nuclear quadrupole coupling constants (NQCC). Specifically, the electronic configuration around the quadrupolar nucleus can be evaluated, determining the nature of the chemical bond in which it participates.[30–33] For instance, a comparison of the ^{14}N, ^{35}Cl, and ^{37}Cl NQCC of NH_3HCl to those of NH_3 and HCl has unambiguously shown that NH_3HCl forms a hydrogen-bonded binary complex in the gas phase rather than an ionic pair as $NH_4^+Cl^-$.[34]

In tandem with experimental characterizations of microhydrates, accurate theoretical predictions of spectroscopic constants can significantly ease the difficulties in assignments and aid the interpretations of observations. As is well known, MW spectroscopy provides direct access to rotational constants for the ground vibrational state B_τ^0 with τ representing one of the principal axes of inertia (a, b, c).[35] These constants are subject to non-negligible vibrational averaging effects, which become more pronounced and intricate as the molecular size increases. QC methods have emerged as accurate alternatives for computing these contributions.[35–38] In the framework of vibrational perturbation theory to second order (VPT2),[39–43] vibrational corrections to rotational constants, dipole moments, and quadrupolar coupling constants require harmonic and semi-diagonal cubic force constants along with the first and second derivatives of the property in question.[44] Typically, the contribution of vibrational corrections is well below 1 % of the corresponding equilibrium rotational constants, allowing for their determination at affordable levels of theory, even when a sub-1 % accuracy is sought. Interpretation of MW spectroscopic studies for medium- to large-sized molecules usually rely on geometry optimizations performed with hybrid density functionals or wave-function methods rooted in the second-order Møller-Plesset perturbation theory (MP2), in conjunction with double- or triple-zeta basis sets. The typical accuracy of these methods (around 1 %) justifies the neglect of vibrational correction. Improved results can be obtained by resorting to double-hybrid functionals, whose accuracy can reach 0.3 %, provided that the accompanying basis set is carefully chosen. Of course, in this case vibrational corrections can no longer be neglected.

Mono-ethanolamine (MEA) is a primary amine of atmospheric and astrophysical relevance with attractive chemical properties. It contains one hydroxyl and one amino group, which can both act as hydrogen bond donors and acceptors, likely multiplying possible hydrogen bond networks and binding configurations for the complexes with water. The presence of a ^{14}N quadrupolar nucleus enables the exploration of the nature of the hydrogen bonds in which it is involved, especially as intramolecular and intermolecular O–H···N hydrogen bonds were found in the monomer and the monohydrate, respectively.[45,46] Adding more water molecules could change the balance between intra- and intermolecular O–H···N hydrogen bonds.

Here, we report the rotational spectra of MEA-$(H_2O)_{1–7}$ clusters recorded by both chirped pulse and cavity-enhanced microwave spectrometers. The configurations of these hydrates were identified with the aid of extensive theoretical sampling. For the MEA-$(H_2O)_{1–3}$ clusters, the structures were further confirmed by assignments of singly and doubly ^{18}O substituted isotopologues. Inclusion of vibrational anharmonic contributions led to excellent agreement between experimental results and theoretical predictions. Furthermore, the analysis of the ^{14}N nuclear quadrupole coupling hyperfine structure offered a quantitative measurement on the chemical changes induced by hydration on the amino group, highlighting its progressive transition to a fully hydrated amine.

Methods

Experimental details. The microwave spectra of MEA-water mixtures in the 2–8 GHz frequency range were measured using broadband CP-FTMW[47,48] spectrometers at DESY (Hamburg)[49] and KCL (London).[50,51] For MEA monohydrates and dihydrates, the cavity FTMW spectrometer[52–54] at CQU (Chongqing) was used to measure the transitions in 8–20 GHz with higher resolution. Broadband experiments of the parent species were performed by placing the sample of liquid MEA (98–99 % purity) in an internal reservoir directly attached to the nozzle and heating to 333 K (DESY) or 353 K (KCL). Water was placed in an external reservoir and either heated up to 313 K (DESY) or used without heating at 294 K (KCL). Tests were performed on both instruments, and the temperatures used gave the best spectral intensity. Both instruments used neon at backing pressures of 5 (KCL) or 6 (DESY) bar as a carrier gas to conduct the MEA and water mixture to the vacuum chamber, where it formed a pulsed supersonic jet. In order to isolate the targeted rotational fingerprints of the various MEA hydrates from the complex global spectrum that includes MEA monomers and pure water clusters of various sizes, further measurements were performed at DESY using similar experimental conditions: separate spectra of MEA and pure water were obtained which were then subtracted from the MEA-water spectrum. The measurements of a $H_2{}^{18}O$ enriched sample were taken at KCL and CQU in a similar manner described previously with a 60:40 ratio of $H_2{}^{16}O$: $H_2{}^{18}O$. A full account of the experimental details can be found in the Supporting Information (SI).

Structural sampling. The characterization of binding topologies in MEA-water clusters was performed using a well-established approach, which combines the efficient Conformer-Rotamer Ensemble Sampling Tool (CREST)[55]

for a preliminary exploration of soft degrees of freedom (inter-molecular parameters and intramolecular dihedral angles) with more advanced QC methods for further refinement.[56] The initial exploration was performed at the GFN2-xTB[57] level of theory, which provides a cost-effective means to identify stable isomers. The structures of the most stable species identified at this stage were reoptimized at the B3LYP-D3(BJ)/def2-TZVP[58–60] level (hereafter B3/TZVP) using the ORCA5[61] QC package. The nature (true energy minima) of the final structures and their zero-point energies (ZPEs) were determined by harmonic frequency calculations. The resulting ensemble of low-energy MEA-$(H_2O)_{1–7}$ clusters, within energy windows of 10 to 30 kJ mol^{-1}, can be found in the SI, Tables S1–S6 and Figures S1–S6, together with the corresponding spectroscopic constants, including rotational constants, electric dipole moment components, and ^{14}N NQCC.

Anharmonic calculations. Inclusion of anharmonic vibrational effects is crucial to achieve the necessary accuracy making theoretical data directly comparable to experiments. Within the VPT2 framework, the ground-state vibrational average of a generic property P (P^0) can be written as

$$P^0 = P^{eq} + \Delta P^{vib} \quad (1)$$

where P^{eq} is the corresponding equilibrium value and ΔP^{vib} is the vibrational correction. For a given level of calculation, the contribution of the vibrational correction is usually limited if compared with the corresponding equilibrium value, but its computational cost is in general higher. As a matter of fact, it has become common practice to employ an enhanced level of theory for the calculation of the equilibrium term, while it has been demonstrated that an affordable level of theory (e.g. B3LYP) is sufficient to provide reliable vibrational corrections. The rev-DSD-PBEP86-D3BJ double-hybrid functional[62] (hereafter rDSD) has been employed for the computation of equilibrium geometries and properties. While quadruple-zeta basis sets are usually advocated to reach converged results, partially augmented cc-pVTZ basis sets have been recently proposed as a reasonable compromise between computational cost and accuracy.[63] Improved results at comparable cost can be obtained by the cc-pVTZ-F12 basis set[64] (hereafter 3F12), purposely developed for explicitly correlated computations.[65,66]

On these grounds, spectroscopic parameters such as rotational constants, NQCC, and electric dipole moment components have been computed exploiting the interplay between the rDSD/3F12 and B3LYP/6-31+G* levels of theory, with the resulting model being referred to as rDSD//B3:

$$P^0(\mathrm{rDSD//B3}) = P^{eq}(\mathrm{rDSD/3F12}) + \Delta P^{vib}(\mathrm{B3/6{-}31+G^*}) \quad (2)$$

This strategy ensures a good balance between accuracy and computational cost, particularly as the most demanding part, the calculation of the anharmonic force field required for the vibrational corrections, is performed at an affordable level of theory (B3LYP/6-31+G*). Hence, we applied the anharmonic vibrational calculations using the candidate structures from the structural samplings that match with the experimental assignments as the starting geometries. The corrected rotational constants, electric dipole moment components, and NQCC are summarized in the SI, Tables S7–S26.

Results and Discussion

Spectral assignments. As demonstrated in Figure 1 (a), spectra of ten different MEA-water species were assigned. These spectral signals originate from MEA-$(H_2O)_{1–7}$ clusters, including three monohydrates and two tetrahydrates. All measured transitions were fitted to Watson's Hamiltonian[67] in the A reduction and the I^r representation using the PGOPHER software.[68] The experimental spectroscopic constants of the MEA-$(H_2O)_{1–7}$ main isotopologues are summarized in Tables S27 and S31. For MEA-$(H_2O)_{1–3}$, we also assigned the corresponding $H_2{}^{18}O$ substituted isotopologues, as documented in Tables S28–S30, which allowed the experimental determination of the positions of the water oxygen atoms in these complexes as shown in Figure 1 (b). Furthermore, the ^{14}N quadrupole hyperfine structures arising from the interaction of the electric quadrupole moment of the ^{14}N nucleus with the molecular electric field gradient were resolved for all species. The corresponding PGOPHER files are uploaded at the Zenodo repository.[69]

Structural assignments. Unambiguous assignments of isomer-specific MEA hydration structures were achieved from the comparison of the experimental rotational constants, relative magnitude of dipole moment components, and ^{14}N nuclear quadrupole coupling constants (NQCCs) with their corresponding ground-state theoretical counterparts at the rDSD//B3 level. As shown in Tables S32–S34, an excellent agreement between experimental and theoretical data was achieved, with the experimental rotational constants being reproduced with sub-1 % accuracy. In particular, the accuracy of vibrationally averaged ^{14}N NQCC improved significantly with respect to the results of the B3/TZVP equilibrium geometries. This accentuated the distinctions between structures and allowed discrimination between species with similar rotational constants. As a result, definitive structural assignments were made to the spectral signals of MEA-$(H_2O)_{1–6}$ shown in Figure 1 (b). We found that the previously reported MEA monohydrate spectrum[45,46] was mistakenly assigned to the structure of MEA-H_2O-1. We have reassigned it to the structure of MEA-H_2O-2. The improved methods for structural sampling and spectroscopic constants helped our studies.

In the case of MEA-$(H_2O)_7$, three isoenergetic candidate structures remain indistinguishable even with the aid of rDSD//B3 calculations (Table S34 and Figure S7). These structures share a similar hydration pattern but differ subtly in the orientation of hydrogen atoms—either clockwise or counter-clockwise. For conciseness, our discussion primarily

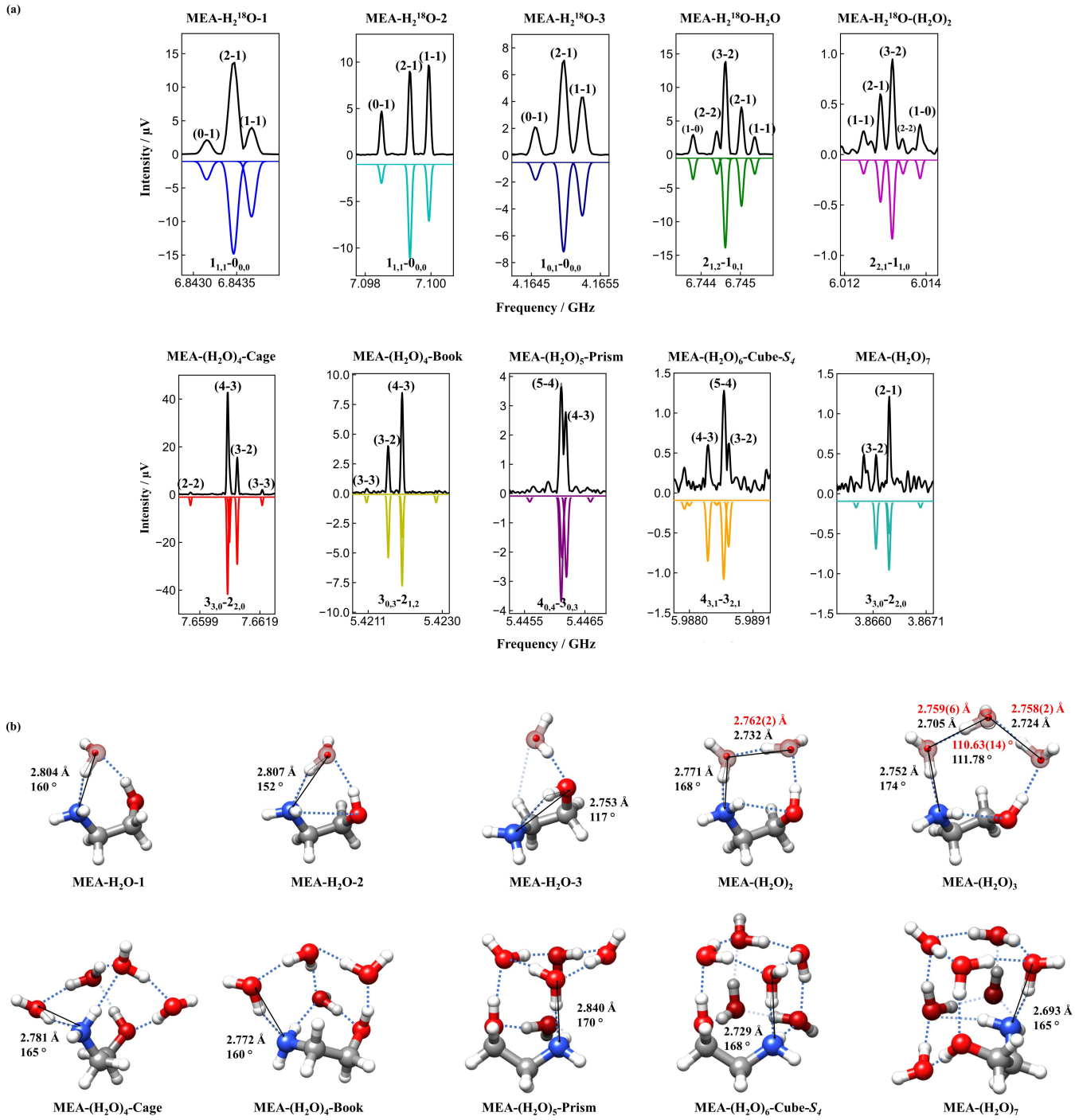

Figure 1. (a) Demonstration of ^{14}N nuclear quadrupole hyperfine transition patterns of singly ^{18}O substituted MEA-$(H_2O)_{1-3}$ and normal species of MEA-$(H_2O)_{4-7}$, with the experimental spectra in the upper trace and the fitted spectra in the lower trace. The rotational transitions are labelled using the standard nomenclature for the rotational energy levels of an asymmetric top, denoted as $J_{Ka,Kc}$. The hyperfine components are labelled with *F'-F''*. *F* is the good quantum number defined as $F = I + J$, where $I = 1$ is the nuclear spin quantum number of ^{14}N. (b) The experimentally identified structures of MEA-water complexes optimized at the B3/TZVP level of theory. In the case of MEA-$(H_2O)_{1-3}$, O···O distances and angles derived from Kraitchman coordinates (in red) are plotted in comparison with these of theory (in black). In addition, the calculated geometry parameters of the O–H···N hydrogen bond including N–O distances and hydrogen bond angles are highlighted in black.

considers the most stable isomer of MEA-$(H_2O)_7$ based on our QC calculations, as depicted in Figure 1 (b). The details are presented in the SI, Tables S32–S34 and Figure S7. In the following, we discuss the size-dependent evolution path of MEA hydrates based on the detected structures.

Evolution of hydration structures and energies. The hydrogen bond networks within the observed MEA-

$(H_2O)_{1-7}$ clusters closely resemble those of the $(H_2O)_{3-9}$ water clusters[13–20] reported before (Figures S8 and S9). In MEA hydrates, each MEA functional group acts as a water molecule, with the capacity of engaging in hydrogen bonds as a donor or an acceptor. In the small MEA-$(H_2O)_{1-3}$ clusters, the binding arrangements typically adopt 2D chain or cyclic configurations, where the MEA moiety forms two hydrogen bonds with water molecules. As the cluster size increases to MEA-$(H_2O)_{4-6}$, the MEA moiety is involved in four hydrogen bonds with water molecules, leading to the formation of 3D networks. These include cage and book structures of MEA-$(H_2O)_4$, a prism structure of MEA-$(H_2O)_5$, and a cube structure of MEA-$(H_2O)_6$. These configurations mimic the arrangements observed for the $(H_2O)_6$, $(H_2O)_7$, and $(H_2O)_8$ water clusters, respectively, as shown in Figures S8 and S9. For all three candidates of MEA-$(H_2O)_7$, both hydrogen atoms of the amino group are involved in the hydrogen bond networks. One hydrogen atom forms a bond with a water molecule, while the other inserts itself within the interior of the hydration cube, establishing a fifth hydrogen bond with neighboring oxygen lone pairs of water molecules.

Furthermore, we performed an energy analysis to evaluate the size-dependent interaction strength between MEA and water molecules. The minimum structures of all identified MEA hydrates, optimized using the B3/TZVP level, were subjected to symmetry-adapted perturbation theory (SAPT) intermolecular binding energy decomposition calculations[70] with the PSI4 software package.[71] The analysis focuses on the total binary binding energies (ΔE_{total}), treating all water molecules as a single collective binding partner and the MEA moiety as the other binding partner in each hydrate (Table S35). For MEA-$(H_2O)_{1-3}$, where MEA establishes two hydrogen bonds with neighboring water molecules, the ΔE_{total} are in the range of 15 to 45 kJ mol^{-1}. After the transition to 3D hydrogen bond networks, the ΔE_{total} of MEA-$(H_2O)_{4-7}$, where four or five hydrogen bonds between MEA and neighboring water molecules are present, further increased up to 152 kJ mol^{-1}.

Hydration-induced conformational changes on the MEA monomer. As illustrated in Figure 2 (a), there are three flexible dihedral angles in the MEA monomer, including the torsional motions of the amino group (Θ_1), the hydroxyl group (Θ_2), and the rotation around the C–C single bond (Θ_3), which regulate the transient chirality of MEA. We performed a relaxed scan of Θ_1 and Θ_2 on the potential energy surface (PES) of the MEA monomer at the B3/TZVP level of theory, identifying eight distinct potential wells, as shown in Figure S10. The minimum energy structures associated with these wells reveal varied intramolecular hydrogen bonding: M1 and M2 feature an O–H···N intramolecular hydrogen bond; M3 to M6 exhibit a weaker N–H···O intramolecular hydrogen bond; and M7 and M8 do not adopt any intramolecular binding configurations. We use the PES of the MEA monomer as a background to demonstrate the hydration induced conformational change of the MEA monomer in Figure 2 (b). Simplified notations on the PES indicate specific MEA hydrates, where the first number is the number of water molecules in the observed MEA-$(H_2O)_n$ complexes, and the second part represents specific structures of the isomers. For example, 1–1 and 4-Cage represent MEA-H_2O-1 and MEA-$(H_2O)_4$-Cage, respectively.

Upon hydration, the non-linear O–H···N intramolecular hydrogen bond (117°) that characterizes the most stable MEA conformer is broken to form more linear O–H···N intermolecular hydrogen bonds (160–174° in Figure 1 (b)) with water molecules, except in the case of MEA-H_2O-3. The conformation of the MEA monomer undergoes significant changes to facilitate the formation of the most energetically favorable hydrogen bond networks. These hydration effects induce a conformational transition in MEA, shifting it from its initial position in the potential well (M1) towards other low energy areas, in particular, the energy valley

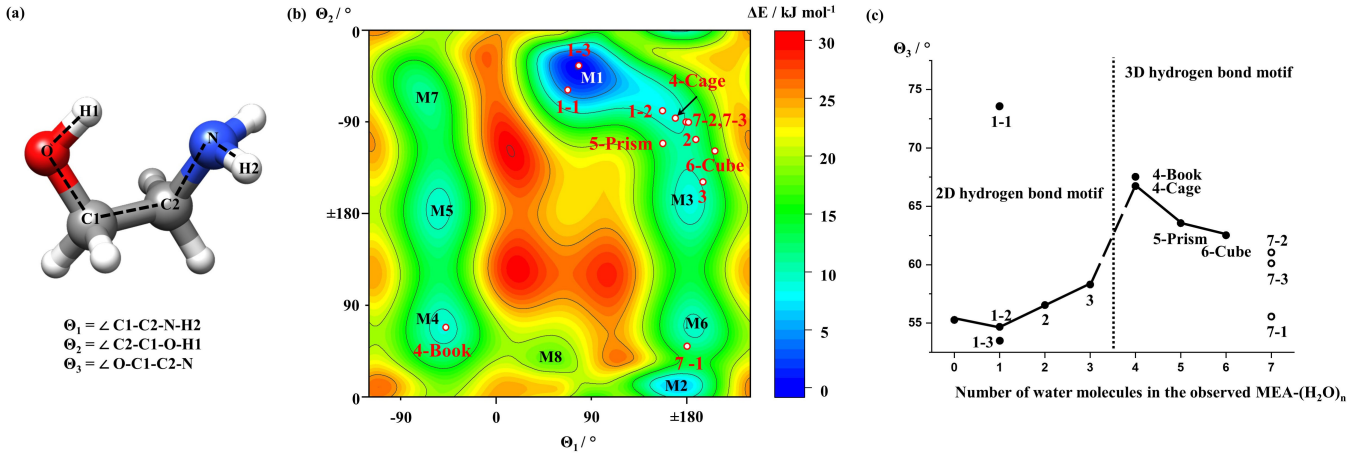

Figure 2. (a) The three flexible dihedral angles of the MEA monomer including the torsional degree of freedom of NH_2 (Θ_1), OH (Θ_2), and C–C (Θ_3). (b) Relaxed two-dimensional energy scan along torsional motions of NH_2 (Θ_1) and OH (Θ_2) of the MEA monomer calculated at the B3/TZVP level of theory. Hydration-induced changes of Θ_1 and Θ_2 to the MEA monomers in the observed MEA hydrates are marked on the PES. (c) Hydration induced change of Θ_3 to the MEA monomers in the observed MEA hydrates. For $n=7$, three candidate structures are indicated with hollow circles.

connecting M1 and M3. These transitions involve overcoming barriers ranging from 5 to 15 kJ mol^{-1}, thereby allowing the MEA moiety to adjust its structure according to the PES.

For MEA-H_2O-2, MEA-$(H_2O)_2$, and MEA-$(H_2O)_3$ with 2D cyclic hydrogen bond networks, N–H···O intramolecular hydrogen bonds are formed to enhance the connectivity of the ring (Figure 1 (b)). In MEA-$(H_2O)_{4-7}$ with 3D hydrogen bond networks, these intramolecular hydrogen bonds are broken to accommodate water molecules in between the amine and hydroxyl groups, which opens the Θ_3 angle of MEA starting from $n=4$, as shown in Figure 2 (c). Such conformational changes facilitate the formation of up to five hydrogen bonds between MEA and water molecules.

Correlation between NQCC and strength of hydrogen bonds. The experimental determination of ^{14}N NQCC provides valuable insights into the local electronic environment surrounding the nitrogen atom of the observed MEA hydrates, which is significantly influenced by hydrogen bonds involving the amino group. To achieve a meaningful comparison, we performed a transformation on the ^{14}N NQCC from the principal inertial axis system (a, b, and c) of the molecular frame to the atomic frame of the nitrogen nucleus, known as the quadrupole principal axes system (x, y, and z), in which the z axis is parallel to the lone pair of the amino group.[72–74] This reorientation ensures that the resulting quadrupole coupling tensor is diagonal, with the diagonal elements χ_{xx}, χ_{yy}, and χ_{zz} reflecting the electron densities on the C–N bond, N–H bonds, and the lone pair of the amino group, respectively. However, the off-diagonal elements of the ^{14}N NQCC in the principal inertial axis frame remain experimentally undetermined due to their weak effect on the spectra. We adopted their vibrationally averaged values calculated at the rDSD//B3 level and incorporated a 5 % error bar based on the average accuracy of the calculated diagonal elements in the rotation of matrices. Hence, the resulting ^{14}N NQCC in the nitrogen nucleus frame are quasi-experimental. The analysis was performed across all the identified MEA hydrates. The detailed outputs and visualizations are summarized in the SI.

Interestingly, a notable correlation emerged between the quasi-experimental χ_{zz} values and the calculated N···O distance as shown in Figure 3. A less negative value of χ_{zz} corresponds to a shorter N···O distance, indicating a stronger O–H···N intermolecular hydrogen bond. The error bar weighted correlation coefficient (ρ) between these two quantities is determined to be −0.96, excluding MEA-H_2O-3. The correlation decreased significantly to −0.86 when MEA-H_2O-3 was included as illustrated in Figure S11. However, the N···O distance in MEA-H_2O-3 does not represent the relative strength of the intermolecular hydrogen bond as in other MEA hydrates, since the O–H···N bond in MEA-H_2O-3 is an intramolecular hydrogen bond and the MEA geometry constraints the ∠OHN angle to be much smaller (117° vs. 150–170°, see Figure 1a).

Our analysis thus demonstrates a robust and close correlation between χ_{zz} and the N···O distance of the intermolecular hydrogen bonds with similar angles. Notably,

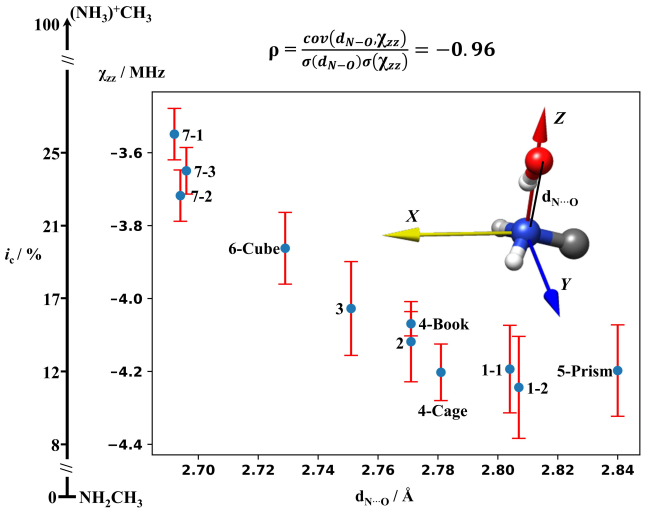

Figure 3. The correlation between $d_{N\cdots O}$ and χ_{zz} on the detected MEA hydrates, except MEA-H_2O-3. $d_{N\cdots O}$ is taken from the minimum geometries optimized at the B3/TZVP level of theory. χ_{zz} is taken from the diagonalized ^{14}N quadrupole coupling tensors. The error bar weighted correlation coefficient between these two parameters is −0.96. The corresponding ionic characters (i_c) are plotted in parallel to the values of χ_{zz}.

the χ_{zz} values of the three heptahydrate candidates were found to be the least negative among all observed hydrates. This indicates that a further reinforced O–H···N intermolecular hydrogen bond arose from better connectivity and higher cooperativity of the hydrogen bond network is formed in heptahydrates.

Furthermore, in the spirit of the Townes-Dailey analysis,[72–74] we propose the following expression for the ionic character (i_c) of a primary amine under conditions of microhydration:

$$i_c = 1 - \frac{\chi_{zz}}{\chi_0} \tag{3}$$

Here, χ_0 is the NQCC along the lone pair direction of methylamine, determined as −4.795(27) MHz.[75] It reflects the electronic configuration of the amino group without hydrogen bonds. This definition gives an i_c of zero for methylamine in the gas phase, and an i_c of one for a protonated methylamine (χ_{zz} ~0.1 MHz) that would present a fully ionized primary amine in the aqueous solution. In the case of the detected MEA-water complexes, microsolvation with up to seven water molecules induced up to 27 % ionicity towards the formation of a protonated amine. This range indicates a gradual transition towards the formation of a protonated amine, highlighting the significant role of hydration in altering a primary amine's intrinsic electronic structure.

Conclusions

The synergistic use of rotational spectroscopy and theoretical modeling provided unambiguous identifications of MEA microhydrates with up to seven water molecules. Upon hydration, the MEA molecule undergoes considerable conformational adjustments to align with the most energetically favorable hydrogen bond motifs, which closely mirror those found in pure water clusters. By focusing on the analysis of ^{14}N NQCC, we have successfully established a robust correlation between the quasi-experimental χ_{zz} and the strength of the hydrogen bond along the lone pair direction of the amino group. This relationship underscores the utility of NQCC as a distinctive marker of hydration levels in amino groups.

More specifically, in the case of MEA heptahydrates, we observed approximately 21–27 % ionicity, indicating a significant shift towards the formation of a protonated amine. These changes demonstrated the effects of microhydration on the electronic environment of an amino group, potentially impacting future studies on amine hydration dynamics in atmospheric chemistry and biological systems. Our research does not only enhance the understanding of MEA hydration but also contributes to broader applications in understanding amine reactivity and interaction patterns in various scientific domains.

Acknowledgements

M. S. and F. X. acknowledge financial support by the Deutsche Forschungsgemeinschaft in the context of the priority program SPP1807 (SCHN1280/4-2). F. X. acknowledges the support of the Alexander von Humboldt postdoctoral fellowship. M.M. and V.B. acknowledge the financial support of a R&D grant of Gaussian Inc. W.O., S. I. M. and M.E.S thank funding from the Royal Society (IEC\NSFC \181109) and King's College London. They also acknowledge use of the high-performance computing cluster CREATE (King's Computational Research, Engineering and Technology Environment). Q. G. and J. L. are grateful for support from the National Natural Science Foundation of China (Grant No. 22073013) and Chongqing Talents: Exceptional Young Talents Project (Grant No. cstc2021ycjh-bgzxm0027). Open Access funding enabled and organized by Projekt DEAL.

Conflict of Interest

The authors declare no conflict of interest.

Data Availability Statement

The data that support the findings of this study are available from the corresponding author upon reasonable request.

Keywords: Hydrogen bond · Rotational spectroscopy · Microhydration · Nuclear quadrupole coupling · Conformations

[1] W. P. Jencks, *Chem. Rev.* **1972**, *72* (6), 705–718, https://doi.org/10.1021/cr60280a004.
[2] M. J. Tait, F. Franks, *Nature* **1971**, *230*, 91–94. https://doi.org/10.1038/230091a0.
[3] C.-J. Li, L. Chen, *Chem. Soc. Rev.* **2006**, *35* (1), 68–82, https://doi.org/10.1039/B507207G.
[4] O. F. Mohammed, D. Pines, J. Dreyer, E. Pines, E. T. J. Nibbering, *Science* **2005**, *310* (5745), 83–86, https://doi.org/10.1126/science.1117756.
[5] E. Persch, O. Dumele, F. Diederich, *Angew. Chem. Int. Ed.* **2015**, *54* (11), 3290–3327, https://doi.org/10.1002/anie.201408487.
[6] D. M. Cwiertny, M. A. Young, V. H. Grassian, *Annu. Rev. Phys. Chem.* **2008**, *59* (1), 27–51, https://doi.org/10.1146/annurev.physchem.59.032607.093630.
[7] M. Shiraiwa, M. Ammann, T. Koop, U. Pöschl, *Proc. Natl. Acad. Sci. USA* **2011**, *108* (27), 11003–11008, https://doi.org/10.1073/pnas.1103045108.
[8] M. S. Cheung, A. E. García, J. N. Onuchic, *Proc. Natl. Acad. Sci. USA* **2002**, *99* (2), 685–690, https://doi.org/10.1073/pnas.022387699.
[9] R. Zhou, X. Huang, C. J. Margulis, B. J. Berne, *Science* **2004**, *305* (5690), 1605–1609, https://doi.org/10.1126/science.1101176.
[10] B. Jayaram, T. Jain, *Annu. Rev. Biophys. Biomol. Struct.* **2004**, *33* (1), 343–361, https://doi.org/10.1146/annurev.biophys.33.110502.140414.
[11] P. F. Bernath, *Phys. Chem. Chem. Phys.* **2002**, *4* (9), 1501–1509, https://doi.org/10.1039/b200372d.
[12] K. R. Leopold, *Annu. Rev. Phys. Chem.* **2011**, *62* (1), 327–349, https://doi.org/10.1146/annurev-physchem-032210–103409.
[13] Z. S. Huang, R. E. Miller, *J. Chem. Phys.* **1989**, *91* (11), 6613–6631, https://doi.org/10.1063/1.457380.
[14] R. S. Fellers, C. Leforestier, L. B. Braly, M. G. Brown, R. J. Saykally, *Science* **1999**, *284* (5416), 945–948, https://doi.org/10.1126/science.284.5416.945.
[15] J. D. Cruzan, L. B. Braly, K. Liu, M. G. Brown, J. G. Loeser, R. J. Saykally, *Science* **1996**, *271* (5245), 59–62, https://doi.org/10.1126/science.271.5245.59.
[16] K. Liu, M. G. Brown, J. D. Cruzan, R. J. Saykally, *Science* **1996**, *271* (5245), 62–64, https://doi.org/10.1126/science.271.5245.62.
[17] C. Pérez, M. T. Muckle, D. P. Zaleski, N. A. Seifert, B. Temelso, G. C. Shields, Z. Kisiel, B. H. Pate, *Science* **2012**, *336* (6083), 897–901, https://doi.org/10.1126/science.1220574.
[18] C. Pérez, S. Lobsiger, N. A. Seifert, D. P. Zaleski, B. Temelso, G. C. Shields, Z. Kisiel, B. H. Pate, *Chem. Phys. Lett.* **2013**, *571*, 1–15, https://doi.org/10.1016/j.cplett.2013.04.014.
[19] W. T. S. Cole, J. D. Farrell, D. J. Wales, R. J. Saykally, *Science* **2016**, *352* (6290), 1194–1197, https://doi.org/10.1126/science.aad8625.
[20] C. Pérez, D. P. Zaleski, N. A. Seifert, B. Temelso, G. C. Shields, Z. Kisiel, B. H. Pate, *Angew. Chem. Int. Ed.* **2014**, *53* (52), 14368–14372, https://doi.org/10.1002/anie.201407447.
[21] S. Blanco, P. Pinacho, J. C. López, *J. Phys. Chem. Lett.* **2017**, *8* (24), 6060–6066, https://doi.org/10.1021/acs.jpclett.7b02948.
[22] C. Pérez, J. L. Neill, M. T. Muckle, D. P. Zaleski, I. Peña, J. C. Lopez, J. L. Alonso, B. H. Pate, *Angew. Chem.* **2015**, *127* (3), 993–996, https://doi.org/10.1002/ange.201409057.
[23] W. Sun, M. Schnell, *Angew. Chem. Int. Ed.* **2022**, *61* (49), e202210819, https://doi.org/10.1002/anie.202210819.
[24] A. L. Steber, B. Temelso, Z. Kisiel, M. Schnell, C. Pérez, *Proc. Natl. Acad. Sci. USA* **2023**, *120* (9), e2214970120, https://doi.org/10.1073/pnas.2214970120.

[25] W. Li, C. Pérez, A. L. Steber, M. Schnell, D. Lv, G. Wang, X. Zeng, M. Zhou, *J. Am. Chem. Soc* **2023**, *145* (7), 4119–4128, https://doi.org/10.1021/jacs.2c11732.
[26] S. Baweja, S. Panchagnula, M. E. Sanz, L. Evangelisti, C. Pérez, C. West, B. H. Pate, *J. Phys. Chem. Lett.* **2022**, *13* (40), 9510–9516, https://doi.org/10.1021/acs.jpclett.2c02618.
[27] A. S. Hazrah, A. Insausti, J. Ma, M. H. Al-Jabiri, W. Jäger, Y. Xu, *Angew. Chem. Int. Ed.* **2023**, *62* (44), e202310610, https://doi.org/10.1002/anie.202310610.
[28] E. Burevschi, M. Chrayteh, S. I. Murugachandran, D. Loru, P. Dréan, M. E. Sanz, *J. Am. Chem. Soc* **2024**, *146* (15), 10925–10933, https://doi.org/10.1021/jacs.4c01891.
[29] S. Saxena, E. Burevschi, Y. Zheng, Q. Gou, M. E. Sanz, *ISMS* **2020**. DOI: 10.15278/isms.2020.WE01.
[30] A. C. Legon, *Chem. Soc. Rev.* **1993**, *22* (3), 153–163, https://doi.org/10.1039/cs9932200153.
[31] A. C. Legon, C. A. Rego, *Chem. Phys. Lett.* **1989**, *162* (4–5), 369–375, https://doi.org/10.1016/0009-2614(89)87060–5.
[32] F. H. De Leeuw, R. Van Wachem, A. Dymanus, *J. Chem. Phys.* **1970**, *53* (3), 981–984, https://doi.org/10.1063/1.1674166.
[33] A. Mizoguchi, Y. Ohshima, Y. Endo, *J. Chem. Phys.* **2011**, *135* (6), 064307, https://doi.org/10.1063/1.3616047.
[34] N. W. Howard, A. C. Legon, *J. Chem. Phys.* **1988**, *88* (8), 4694–4701, https://doi.org/10.1063/1.453783.
[35] C. Puzzarini, J. F. Stanton, J. Gauss, *Int. Rev. Phys. Chem.* **2010**, *29* (2), 273–367, https://doi.org/10.1080/01442351003643401.
[36] J. Demaison, *Mol. Phys.* **2007**, *105* (23–24), 3109–3138, https://doi.org/10.1080/00268970701765811.
[37] M. Mendolicchio, E. Penocchio, D. Licari, N. Tasinato, V. Barone, *J. Chem. Theory Comput.* **2017**, *13* (6), 3060–3075, https://doi.org/10.1021/acs.jctc.7b00279.
[38] V. Barone, *Phys. Chem. Chem. Phys.* **2024**, *26* (7), 5802–5821, https://doi.org/10.1039/D3CP05169B.
[39] H. H. Nielsen, *Rev. Mod. Phys.* **1951**, *23* (2), 90–136, https://doi.org/10.1103/RevModPhys.23.90.
[40] M. Mendolicchio, J. Bloino, V. Barone, *J. Chem. Theory Comput.* **2021**, *17* (7), 4332–4358, https://doi.org/10.1021/acs.jctc.1c00240.
[41] Q. Yang, M. Mendolicchio, V. Barone, J. Bloino, *Front. Astron. Space Sci.* **2021**, *8*, 665232, https://doi.org/10.3389/fspas.2021.665232.
[42] P. R. Franke, J. F. Stanton, G. E. Douberly, *J. Phys. Chem. A* **2021**, *125* (6), 1301–1324, https://doi.org/10.1021/acs.jpca.0c09526.
[43] M. Mendolicchio, *Theor. Chem. Acc.* **2023**, *142* (12), 133, https://doi.org/10.1007/s00214-023–03069-7.
[44] V. Barone, *J. Chem. Phys.* **2005**, *122* (1), 014108, https://doi.org/10.1063/1.1824881.
[45] S. L. Widicus, B. J. Drouin, K. A. Dyl, G. A. Blake, *J. Mol. Spectrosc.* **2003**, *217* (2), 278–281, https://doi.org/10.1016/S0022-2852(02)00056–5.
[46] M. J. Tubergen, C. R. Torok, R. J. Lavrich, *J. Chem. Phys.* **2003**, *119* (16), 8397–8403, https://doi.org/10.1063/1.1612919.
[47] G. G. Brown, B. C. Dian, K. O. Douglass, S. M. Geyer, B. H. Pate, *J. Mol. Spectrosc.* **2006**, *238* (2), 200–212, https://doi.org/10.1016/j.jms.2006.05.003.
[48] G. G. Brown, B. C. Dian, K. O. Douglass, S. M. Geyer, S. T. Shipman, B. H. Pate, *Rev. Sci. Instrum.* **2008**, *79* (5), 053103, https://doi.org/10.1063/1.2919120.
[49] D. Schmitz, V. Alvin Shubert, T. Betz, M. Schnell, *J. Mol. Spectrosc.* **2012**, *280*, 77–84, https://doi.org/10.1016/j.jms.2012.08.001.
[50] D. Loru, M. A. Bermúdez, M. E. Sanz, *J. Chem. Phys.* **2016**, *145* (7), 074311, https://doi.org/10.1063/1.4961018.
[51] D. Loru, I. Peña, M. E. Sanz, *J. Mol. Spectrosc.* **2017**, *335*, 93–101, https://doi.org/10.1016/j.jms.2017.03.007.
[52] T. J. Balle, W. H. Flygare, *Rev. Sci. Instrum.* **1981**, *52* (1), 33–45, https://doi.org/10.1063/1.1136443.
[53] J.-U. Grabow, W. Stahl, H. Dreizler, *Rev. Sci. Instrum.* **1996**, *67* (12), 4072–4084, https://doi.org/10.1063/1.1147553.
[54] J. Chen, Y. Zheng, J. Wang, G. Feng, Z. Xia, Q. Gou, *J. Chem. Phys.* **2017**, *147* (9), 094301, https://doi.org/10.1063/1.4994865.
[55] P. Pracht, F. Bohle, S. Grimme, *Phys. Chem. Chem. Phys.* **2020**, *22* (14), 7169–7192.
[56] V. Barone, M. Fusè, F. Lazzari, G. Mancini, *J. Chem. Theory Comput.* **2023**, *19* (4), 1243–1260, https://doi.org/10.1021/acs.jctc.2c01143.
[57] C. Bannwarth, S. Ehlert, S. Grimme, *J. Chem. Theory Comput.* **2019**, *15* (3), 1652–1671, https://doi.org/10.1021/acs.jctc.8b01176.
[58] S. Grimme, S. Ehrlich, L. Goerigk, *J. Comput. Chem.* **2011**, *32* (7), 1456–1465, https://doi.org/10.1002/jcc.21759.
[59] E. Caldeweyher, S. Ehlert, A. Hansen, H. Neugebauer, S. Spicher, C. Bannwarth, S. Grimme, *J. Chem. Phys.* **2019**, *150* (15), 154122, https://doi.org/10.1063/1.5090222.
[60] C. Lee, W. Yang, R. G. Parr, *Phys. Rev. B* **1988**, *37* (2), 785–789, https://doi.org/10.1103/PhysRevB.37.785.
[61] F. Neese, *WIREs Comput. Mol. Sci.* **2022**, *12* (5), e1606, https://doi.org/10.1002/wcms.1606.
[62] G. Santra, N. Sylvetsky, J. M. L. Martin, *J. Phys. Chem. A* **2019**, *123* (24), 5129–5143, https://doi.org/10.1021/acs.jpca.9b03157.
[63] G. Ceselin, V. Barone, N. Tasinato, *J. Chem. Theory Comput.* **2021**, *17* (11), 7290–7311, https://doi.org/10.1021/acs.jctc.1c00788.
[64] K. A. Peterson, T. B. Adler, H.-J. Werner, *J. Chem. Phys.* **2008**, *128* (8), 084102, https://doi.org/10.1063/1.2831537.
[65] V. Barone, *J. Phys. Chem. Lett.* **2023**, *14* (25), 5883–5890, https://doi.org/10.1021/acs.jpclett.3c01380.
[66] V. Barone, *J. Chem. Phys.* **2023**, *159* (8), 081102, https://doi.org/10.1063/5.0167296.
[67] W. Gordy, R. L. Cook, *Microwave Molecular Spectra*; Chemical applications of spectroscopy; Interscience Pub., **1970**.
[68] C. M. Western, *J. Quant. Spectrosc. Radiat. Transfer* **2017**, *186*, 221–242, https://doi.org/10.1016/j.jqsrt.2016.04.010.
[69] Transition Lists/Pgopher Files for Ethanolamine-Water Complexes, https://zenodo.org/records/11519872.
[70] K. Szalewicz, *WIREs Comput. Mol. Sci.* **2012**, *2* (2), 254–272.
[71] D. G. Smith, L. A. Burns, A. C. Simmonett, R. M. Parrish, M. C. Schieber, R. Galvelis, P. Kraus, H. Kruse, R. Di Remigio, A. Alenaizan, *J. Chem. Phys.* **2020**, *152* (18).
[72] C. H. Townes, B. P. Dailey, *J. Chem. Phys.* **1949**, *17* (9), 782–796, https://doi.org/10.1063/1.1747400.
[73] B. P. Dailey, C. H. Townes, *J. Chem. Phys.* **1955**, *23* (1), 118–123, https://doi.org/10.1063/1.1740508.
[74] S. E. Novick, *J. Mol. Spectrosc.* **2011**, *267* (1–2), 13–18, https://doi.org/10.1016/j.jms.2011.01.004.
[75] M. Kréglewski, G. Wlodarczak, *J. Mol. Spectrosc.* **1992**, *156* (2), 383–389, https://doi.org/10.1016/0022-2852(92)90239-K.

Manuscript received: May 7, 2024
Accepted manuscript online: July 10, 2024
Version of record online: September 2, 2024